Biomedical Engineering Letters (2023) 13:729–737
https://doi.org/10.1007/s13534-023-00290-y

ORIGINAL ARTICLE

Skin pore imaging using spectral-domain optical coherence tomography: a case report

Hyunmo Kim[1] · Dongwan Kang[1] · Daewoon Seong[1] · Sm Abu Saleah[1] · Jannat Amrin Luna[1] · Yoonseok Kim[1] · Hayoung Kim[1] · Sangyeob Han[1,2] · Mansik Jeon[1] · Jeehyun Kim[1]

Received: 1 April 2023 / Revised: 15 May 2023 / Accepted: 25 May 2023 / Published online: 3 July 2023

Abstract

Sebum is an important component of the skin that has attracted attention in many fields, including dermatology and cosmetics. Pore expansion due to sebum on the skin can lead to various problems. Therefore, it is necessary to analyze the morphological characteristics of sebum. In this study, we used optical coherence tomography (OCT) to evaluate facial sebum areas. We obtained the OCT maximum amplitude projection (MAP) image and a cross-sectional image of skin pores in the facial area. Subsequently, we detected the sebum in skin pores using the detection algorithm of the ImageJ software to quantitatively determine the size of randomly selected pores in the proposed MAP images. Additionally, the pore size was analyzed by acquiring images before and after facial sebum extraction. According to our research, facial sebum can be morphologically described using the OCT system. Since OCT imaging enables specific analysis of skin parameters, including pores and sebum, skin analysis employing OCT could be an effective method for further research.

Keywords Facial skin pore · Spectral-domain optical coherence tomography (SD-OCT) · Sebum extraction · Image processing · Cross-sectional image

1 Introduction

As the outermost organ of the body, the human skin is a multilayered structure that forms the main interface with the environment [1]. The skin is largely composed of three layers called the epidermis, dermis, and hypodermis [2]. Skincare is crucial because the skin protects the body from the environment, including heat, sunlight, and cold [3]. Numerous skin characteristics, including wrinkles, blackheads, roughness, and texture, have been studied; among these, skin pores are a crucial component in skin surface analysis [4, 5]. The term "skin pores" refers to the expanded openings in the hair follicles on the surface of the skin [6]. The size of skin pores where hair and sebum are present may vary depending on internal and external factors, such as aging or sebum secretion, and many of them are also distributed around the nose [7, 8]. Additionally, when the internal structure of the skin changes, the structure of the skin surface around pores also changes, which leads to a change in pore sizes [9]. As such, the pore sizes differ under various conditions, and several studies have been conducted to objectively and quantitatively analyze pore size [6–10]. Therefore, it is crucial to examine pores of various sizes and shapes.

Facial pores have been evaluated using various methods, such as the visual evaluation method of the distribution and size of pores and optimal image analysis of the number and size of pores [11–13]. Also, many studies have been conducted in the fields of medical skin research and computer animation for detecting changes in skin structure [14–16]. Generally, high-resolution photos with different filters and polarizations have been commonly used to evaluate fine lines, wrinkles, scars, skin tone, pigmentation, and clogged pores.

Hyunmo Kim, Dongwan Kang and Daewoon Seong have contributed equally to this work.

✉ Mansik Jeon
msjeon@knu.ac.kr

✉ Jeehyun Kim
jeehk@knu.ac.kr

[1] School of Electronic and Electrical Engineering, College of IT Engineering, Kyungpook National University, Daegu 41566, Republic of Korea

[2] School of Medicine, Institute of Biomedical Engineering, Kyungpook National University, Daegu 41566, Republic of Korea

Among optical imaging technologies for skin investigation, ultrasound imaging, reflection confocal microscopy (RCM), fluorescence microscopy, and Phase Shift Rapid In Vivo Measurement of Skin (PRIMOS) have been used as useful tools for skin analysis [17–20]. Ultrasound imaging can be performed at millimeter depths noninvasively, but its resolution is limited to approximately 50 μm [5, 21]. Alternatively, RCM and fluorescence microscopy can provide images showing cellular changes in high contrast, but these techniques have the limitations of a narrow field of view and a shallow penetration depth [10, 22]. Moreover, the need to use a fluorescent substance is another limitation of fluorescence microscopy. Finally, an imaging system commonly used for skin measurements, PRIMOS (Canfield, USA), can provide noninvasive, fast, and accurate measurements of the skin surface for analysis of, for example, skin topography and the number of wrinkles [23]. However, the results of PRIMOS depend on the subject's orientation, motion artifacts, and backscatter, which makes accurate and reliable skin analysis challenging [24]. Therefore, a noninvasive and high-resolution optical imaging technique is required to assess skin sebum efficiently.

Optical coherence tomography (OCT) is a noninvasive, high-resolution imaging technique that provides real-time and three-dimensional (3D) morphological information about biological tissues [25–27]. This technique is characterized by high resolution (1–15 μm) in imaging depths from sub-millimeter to millimeter scale (0.3–2 mm), which means that OCT can detect microscopic internal structures [28, 29]. OCT has been widely used in multiple fields, such as ophthalmology [30, 31], otolaryngology [32–35], dentistry [36–38], and even agriculture [39, 40]. Additionally, the combination of interference signals generated via high-sensitivity spectroscopy detection can provide potentially comprehensive information about biological tissues through precise morphological visualization of the samples. Moreover, studies using OCT to examine skin pores without removing tissue have been conducted [41–43]. In particular, high-resolution OCT techniques, such as micro-OCT [44–46], are promising tools to guide the detailed morphological evaluation of sebaceous glands in clinical settings to investigate disease mechanisms and therapeutic targets.

In this study, we developed a SD-OCT system to noninvasively image the skin and quantify the areas of pores and sebum. The USFA 1951 resolution target was used to measure lateral resolution to quantitatively evaluate the performance of the SD-OCT system. Using the proposed system, we obtained a 3D maximum amplitude projection (MAP) image and two-dimensional (2D) cross-sectional images of skin pores, including the sebum. A pore detection algorithm in ImageJ software was used to quantitatively measure the size of selected pores on the MAP images. Additionally, we evaluated the pore size before and after sebum extraction from the nose area. Our findings will potentially be a basic proposal for further studies on skin sebum.

2 Materials and methods

2.1 Development of spectral-domain OCT system

The configuration of the SD-OCT system is shown in Fig. 1. The SD-OCT system operates with a SLED light source (EXS210022-02, EXALOS, Switzerland) having a center wavelength of 840 nm and a 50-nm bandwidth, which is also called full width at half maximum (FWHM). The light from the SLED source travels to a 50:50 fiber coupler (TW850R5A2, Thorlabs, USA), which delivers the divided light to the reference arm and sample arm, respectively. The light travels along the sample path through the collimator, one pair of lenses (lens1; AC254-050-B and lens2; AC254-100-B, Thorlabs, USA), and the objective lens (10×M Plan APO, Edmund Optics, USA) in sequence until it reaches the sample. In this process, the collimator collimates the beam, the pair of lenses expands the beam spot size, and the objective lens with a numerical aperture of 0.28 focuses the beam on the mirror. In the reference arm, the collimator, lens 1, and mirror were used, which are the same as the sample arm, to match the optical path length of the sample arm. Additionally, a dispersion compensation block was employed to correct the dispersion difference in the sample and reference arm. Moreover, the software-based dispersion compensation algorithm was applied as a post processing method. The mirror reflects the focused light so that it is backscattered and returned in the direction from which it came.

Additionally, in the sample path, the two-axis galvanometer scanner (GVS002, Thorlabs, USA) is placed to enable

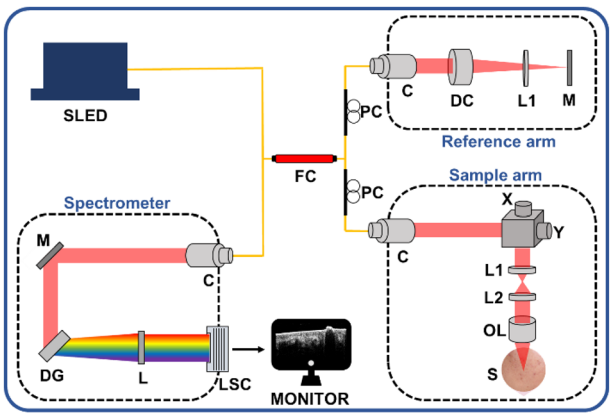

Fig. 1 System configuration of the presented optical coherence tomography (OCT) system to detect the skin pore elements. *C* collimator; *DG* diffraction grating; *FC* fiber coupler; *L* lens; *LSC* line scan camera; *M* mirror; *OL* objective lens; *S* sample; *SLED* super luminescent diode; *PC* polarization controller

raster scanning of the sample. The backscattered beam from both sides of the path (reference and sample) interferes within the fiber coupler and enters the compactly custom-made spectrometer in an aluminum case [47, 48]. The customized version consists of a mirror, a transmission diffraction grating (1800 lines/mm, Wasatch Photonics Inc., USA), an achromatic focusing lens (AC508-100-1B. Thorlabs, USA), and a CMOS line-scan camera with 2048 (H) × 2 (V) pixels (high-speed CMOS camera, spL2048-140 km, Basler, Germany). The diffraction grating disperses the interfered light according to its wavelength. Finally, the focusing lens focuses the dispersed light on the line-scan camera, and a raw signal is detected by the camera.

2.2 Flowchart of system operation

The flow chart of the software program showing the data flow between the CPU and graphics processing unit (GPU) processes and the timing diagram for scanning and image acquisition as presented in Fig. 2. LabVIEW 2017 software was used to display the cross-section (B-scan) for data acquisition. In the developed SD-OCT system, a frame grabber (PCIe-1433, National Instruments, USA) was used to transmit and receive line-scan camera signals. We also utilized Compute Unified Device Architecture (CUDA) through a 2816-core GPU using multithreading (GeForce GTX 980 Ti, NVIDIA, USA) for fast data processing. To remove background noise and nonlinearity in the raw signal, data processing, including background removal, k-linearization (wavenumber linearization), and fast Fourier transform, were applied to the CUDA sub-processor of the GPU. As the final step in GPU processing, log scaling was applied to the data, and the resulting data was sent back to the CPU thread to display the B-scan image in real-time. The frame rate was 50 frames per second; therefore, it took 20 ms to display a single B-scan image. In the present study, 1000 B-scan images were combined, and it took 20 s to acquire MAP (C-scan) images. All OCT B-scan images were reconstructed to generate cross-section, *En-face*, and MAP images.

2.3 Post-processing algorithm for skin pore detection

To detect and analyze skin pore characteristics, a five-step post-processing algorithm for obtaining OCT data was configured in ImageJ (Fig. 3). ImageJ is a freely distributed program based on JAVA and uses simple image-processing technology that analyzes images at the pixel level [49]. Because ImageJ has been used in various scientific studies, such as those on skin structure and internal mitochondrial information, we attempted to analyze the skin OCT data using this tool. First, the Smooth and Gaussian blur filters were used on the original image to clearly distinguish between the skin pores and the rest of the facial features. Subsequently, the location of the pore area was indicated on the optimized image through the "Find Maxima" function

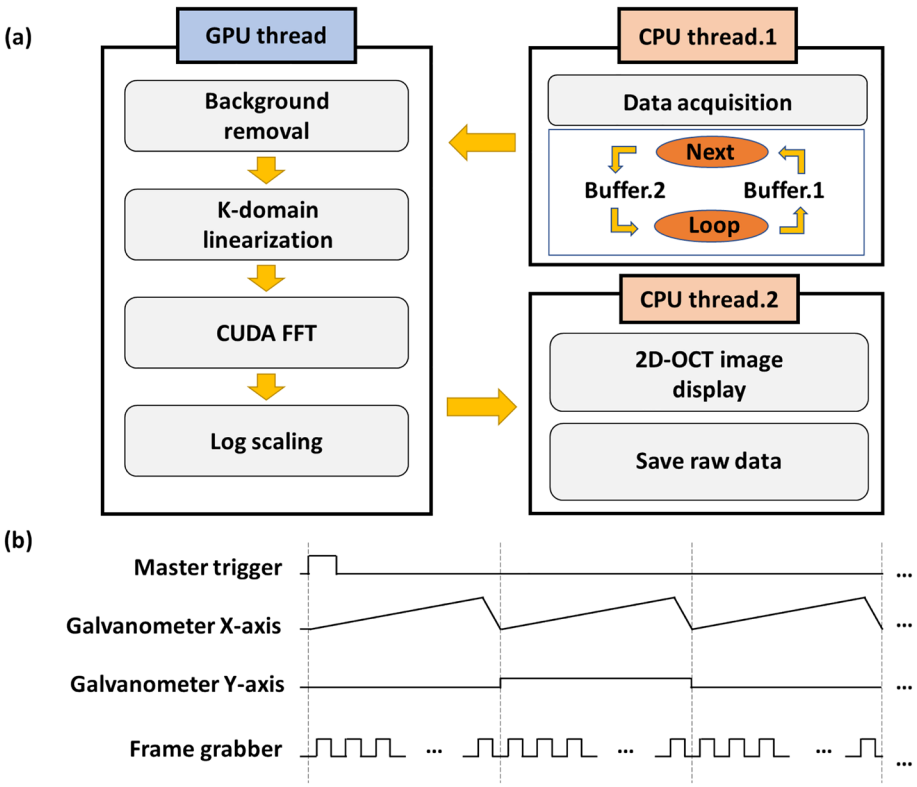

Fig. 2 Description of the flow diagram about the systemic operation. **a** Signal processing in a software part of the OCT **b** A timing diagram showing the scheduling of each hardware component

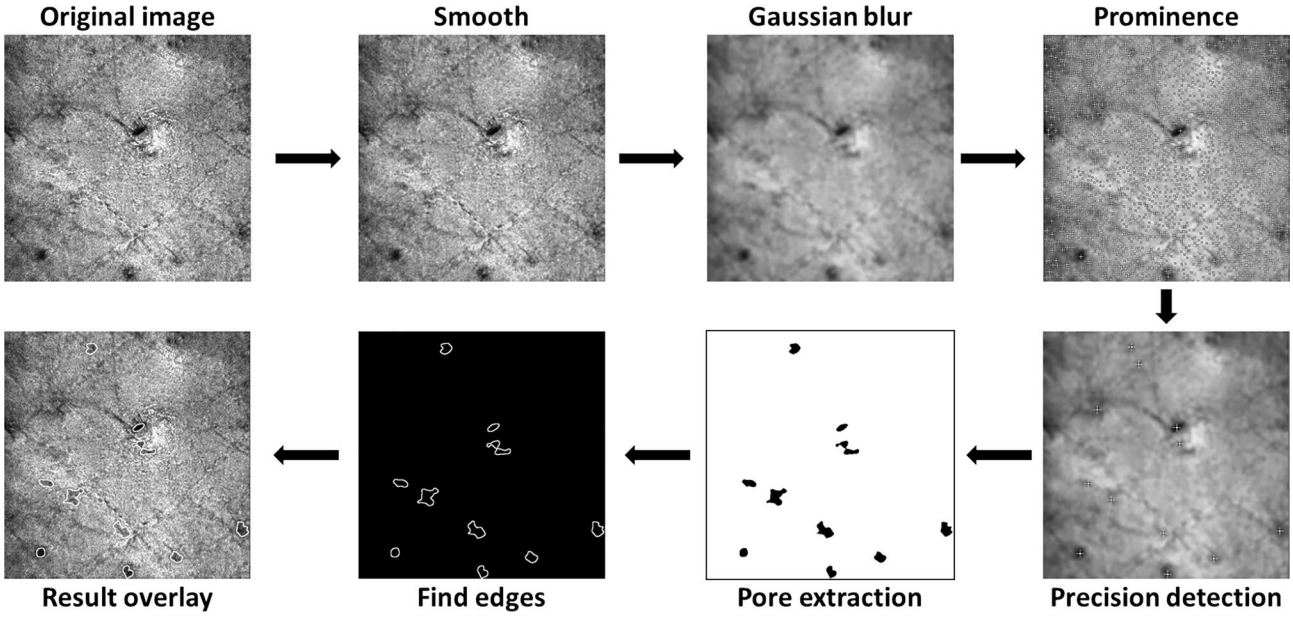

Fig. 3 Process of skin pore detection using the image post-processing method of Image J

installed in ImageJ, as shown in the Prominence part, and precision detection was performed by controlling the numerical value of prominence range. Then pore extraction was performed based on the detected location. Finally, the boundary edge of the extracted area was identified, and the resulting image was derived by overlaying the identified edge on the existing original image. Although the extracted areas contained some other parts except for pores, it was sufficient to detect pores from the acquired OCT MAP data. In the implemented algorithm, quantitative measurement was performed on the resulting data by measuring the size of the facial pores based on the overlaid results. We set sigma (radius) as 3.0 for Gaussian blur, prominence as 46, and using 'exclude edge maxima, light background, and point selection method for precision detection.

3 Results

3.1 Quantitative OCT performance evaluation

To evaluate the performance of the OCT during the experiment, we measured the lateral resolution (Fig. 4). We used the resolution target (USAF 1951, Edmund Optics, USA) and the obtained OCT MAP image, as shown in Fig. 4a. First of all, to perform the intensity profiling, we applied intensity reversal to the image in Fig. 4a, as shown in Fig. 4b, in which group 7 was enlarged. From this image, FWHM intensity fluctuation, corresponding to the lateral resolution, analysis was conducted on element 3 of group 7 of the resolution target in two axes indicated by red-dotted lines (yellow arrows x and y), respectively. As shown in Fig. 4d and e, the intensities in both the x and y axes were accurately extracted from the red dotted line in Fig. 4b. As expressed in each FWHM graph, the three lines on each axis were clearly identified, confirming that the lateral resolution of the developed SD-OCT was about 3.1 µm. Furthermore, the vertical red dotted line in Fig. 4a represents the scanned region, and the cross-sectional image of that portion was obtained, as shown in Fig. 4c.

3.2 Mapping and cross-sectional image of the skin

OCT imaging was performed on the skin of a healthy man in 20 s. During in-vivo human imaging, we used a support that can raise the chin and place the forehead with benchtop type OCT configuration to minimizing the motion-artifact. Representative images obtained during the experiment, including the reconstructed MAP images (left) and cross-sectional images (right), are shown in Fig. 5. As shown in Fig. 5a, the appearance of sebum could be confirmed in the OCT MAP image. The corresponding circles in Fig. 5b, d, f show the cross-sections of the skin sebum, which correspond to the red dashed lines in those Fig. 5a, c, e. The distribution and overall shape of the several sebum are shown in these images. Especially the type of pore to which the hair belongs was also distinguished in the OCT cross-sectional image, as shown in Fig. 5f.

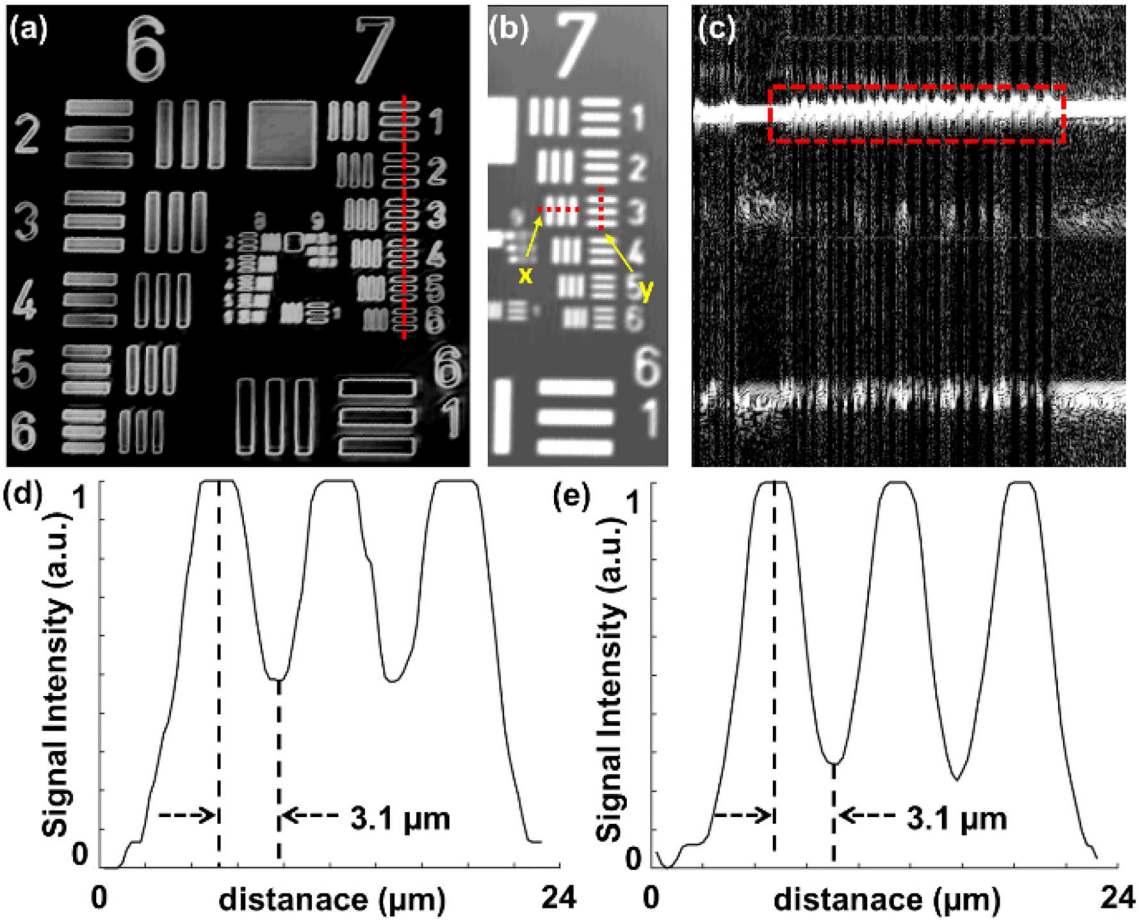

Fig. 4 Performance evaluation of OCT using the resolution target. **a** OCT MAP image of the resolution target focused on 6–7 Groups. **b** Specifically magnified OCT MAP image of the target 7 Group. **c** OCT 2D cross-sectional image that corresponds to the vertical red-dashed line in (**a**). **d**, **e** Resolution analysis using A-scan profiling of each of the x and y axes marked with a red-dotted line in (**b**)

3.3 Applied algorithm and quantitative analysis

Using the obtained OCT MAP data of the skin, we performed quantitative analysis on each pore by applying the developed algorithm. The images were overlaid by adjusting the numerical values for each image in ImageJ (Fig. 6a–c). Facial pores appearing in the original images were almost detected, and area analysis was performed on three representative pores indicated by the red dotted circles in each figure. Nine skin pores with different sizes were arbitrarily selected (comparably large, medium, and small), and the analyze particles function of ImageJ was used to quantitatively measure the size of each part (Table 1). Some pores were detected by dividing them into outer and inner boundaries in the algorithm because of severe reflection caused by sebum during imaging, but the area was measured based on the outer boundary regardless of the inner boundary. The measured pore sizes varied from a maximum of 22.975 mm^2 to a minimum of 1.090 mm^2. In terms of the accuracy of skin pore detection method, there are total 20 skin pore candidates in Fig. 6a–c. Among them, there are 16 real skin pores and others are artifacts on the face surface. Therefore, the calculated accuracy of skin pore detection method is 80%.

3.4 Quantitative analysis before and after skin sebum extraction

Additionally, using the pimple extractor to extract the sebum from the nose, the pore size before and after extraction was compared (Fig. 7). The reconstructed volumetric morphology of the pore in the nose before and after sebum extraction is shown in Fig. 7a and d, respectively. From here, the *en-face* images of these two regions were acquired to analyze the areas in each case (Fig. 7b and e). After applying the implemented algorithm, the area before sebum extraction was quantitatively measured to be approximately 33.705 mm^2, and the area after sebum extraction was approximately 16.879 mm^2 (Table 2). The size of the pore from which sebum was

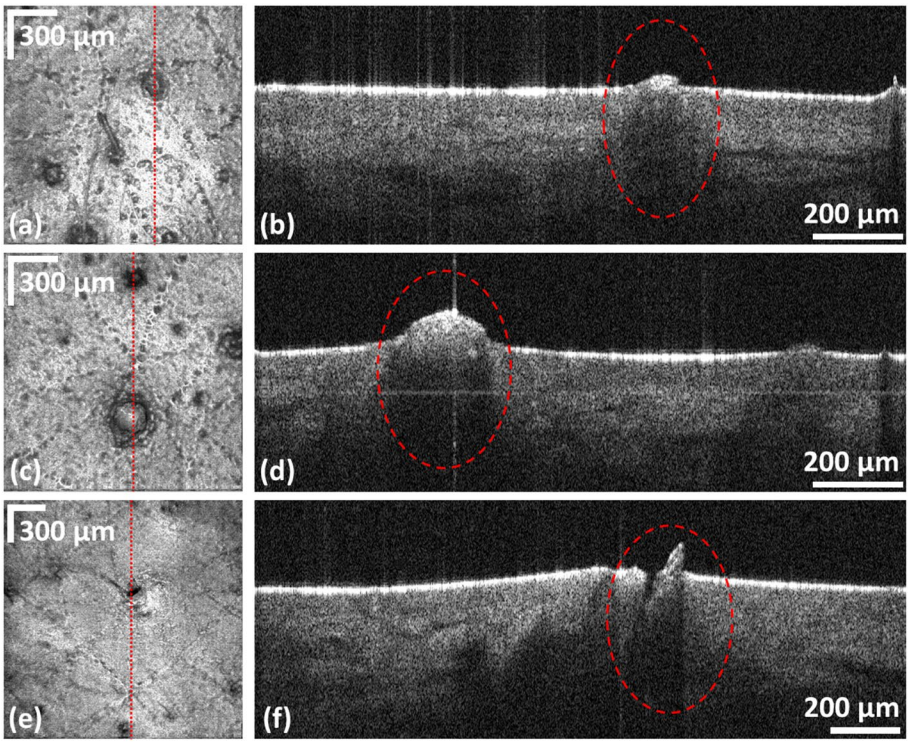

Fig. 5 Skin sebum images were obtained by using OCT. **a**, **c**, **e** MAP OCT images of the skin surface. **b**, **d**, **f** Cross-sectional OCT images were obtained at the vertical red-dashed line in (**a**), (**c**), and (**e**), respectively

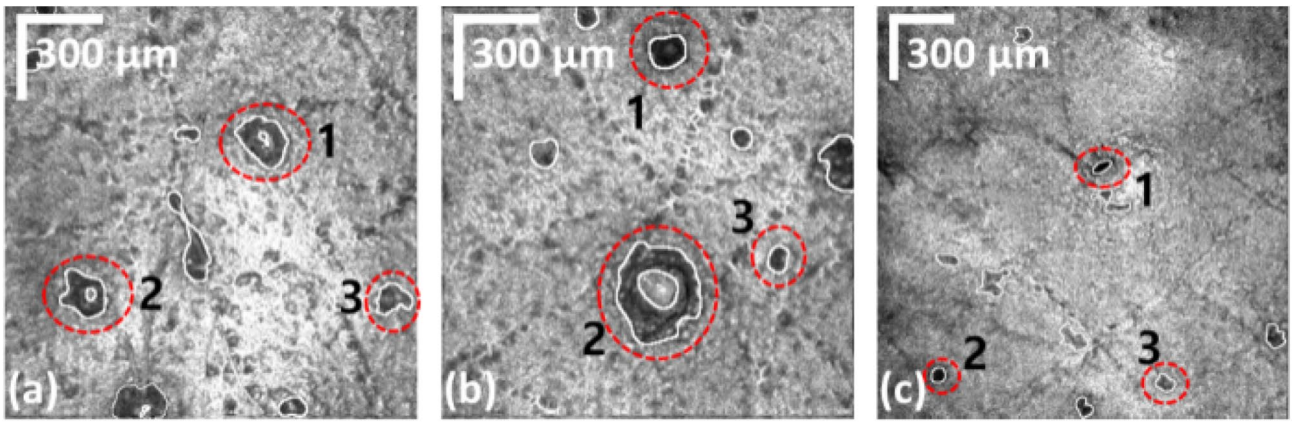

Fig. 6 Quantitative analysis of the red-dotted circle areas in each MAP image **a**–**c** of OCT to which the implemented algorithm was applied

Table 1 Quantitative analysis table of the skin pore areas indicated by red-dotted circles in the above image (a, b, c)

Sebum list (unit)	(a)		(b)		(c)	
	Pixel	mm^2	Pixel	mm^2	Pixel	mm^2
1	1388	6.203	858	3.834	322	2.542
2	1567	7.003	5141	22.98	356	2.811
3	548	2.449	244	1.090	508	4.011

extracted was reduced, and the extraction rate was calculated to be approximately 49.9%. Furthermore, the cross-sectional image of each part was obtained to visualize the extracted part (Fig. 7c and f). These results show that the SD-OCT system can be used to acquire 3D and 2D images for quantitative and qualitative evaluation of the areas before and after sebum extraction.

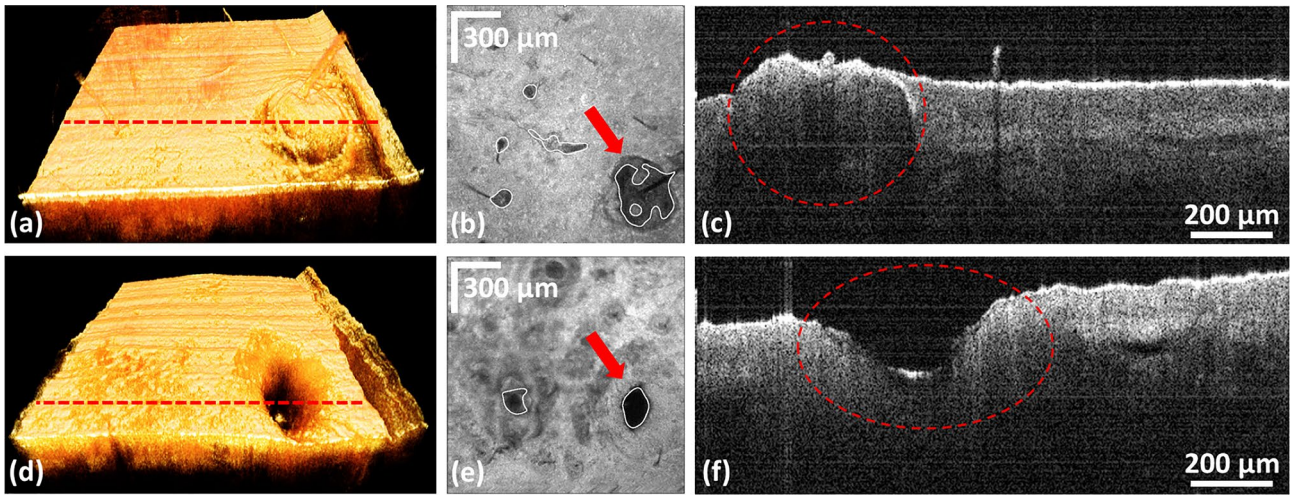

Fig. 7 Comparative analysis of OCT images before and after sebum extraction. **a**, **d** 3D reconstructed skin sebum areas. **b**, **e** *En-face* images of the OCT were reconstructed after using the algorithm. **c**, **f** Cross-sectional OCT images of the sebum area are indicated by the red dotted line in (**a**) and (**d**)

Table 2 Quantitative analysis table of the skin pore areas before and after sebum extraction indicated by red-dotted circles in the above image (b) and image (e)

Sebum extraction (unit)	(a)		(b)	
	Pixel	mm^2	Pixel	mm^2
Area	7542	33.705	3777	16.879
Extracted rate	49.9%			

4 Discussion

OCT is a valuable imaging technique that can perform high-resolution and noninvasive imaging for the measurement of facial skin features. With the development of OCT-related technologies, many studies [50–52] have been conducted on skin features, such as pores, wrinkles, and sweat glands. This study aimed to measure the pore size, including sebum, in three arbitrarily selected cases as a preliminary step in skin sebum research. Since the average size of skin pores shows a rather high variability among ethnic groups, ranging from 0.03 mm^2 to over 1 mm^2 [53], it is required to enhance the lateral resolution of OCT to conduct the quantitative analysis with high accuracy for various sizes of skin pores. Therefore, we enhanced the lateral resolution compared to the conventional OCT to improve the versatility of our proposed method. The measured values before and after sebum extraction were compared. In addition, the selected case proves that OCT-based quantitative analysis is possible through the fact that the extracted area is included in the depth of focus of the used OCT system. Additionally, the implemented area measurement algorithm was suitable for measuring skin pore sizes. Unlike conventional ultrasound imaging, RCM, and fluorescence microscopy, the morphological appearances of the skin could be intuitively visualized using OCT with a label-free feature, high resolution, and a wide field of view. Specifically, OCT has advantages in terms of resolution (higher than ultrasound imaging), the field of view and penetration depth (much wider and deeper than RCM), and labeling (fluorescent substance is required in fluorescence microscopy). In addition, specifically in OCT and PRIMOS comparison, although the imaging speed of PRIMOS is faster than OCT by utilizing the area scan camera, OCT has a distinction in that it can provide high-resolution lateral and depth-direction resolution of internal tomographic structures that PRIMOS cannot provide.

The properties of the optical interference-based OCT system in the present skin sebum study can be further improved. In this study, we preferentially performed area measurements using 3D MAP images, but additional volume analysis using cross-sectional images is required to analyze the morphological characteristics of sebum. To proceed with quantitative volumetric analysis of sebum, the sebum properties can be clearly distinguished by increasing the penetration depth of the system and better revealing the structure of the skin sebum. By adjusting the optical component to increase the penetration depth, the structure in the depth direction of the object can be analyzed closely. Improved penetration depth would enable a volumetric and cross-sectional analysis of skin sebum images obtained with the OCT system in future studies. In addition, in terms of imaging speed, the maximum achievable A-line rate of this system is 100 kHz when considering the acquisition and processing time. In this case, the frame rate of B-scan is able to be increased by 200 fps (100 kHz/500 A-lines) and

one 3D volume is acquired in 5 s (1/100 kHz * 500 A-lines * 1000 B-scans), which enhances the applicability of OCT in clinical fields. Moreover, the imaging speed of OCT is also able to be increased by using the dual camera-based SD-OCT setup [54] or by introducing swept-source OCT. The information obtained in this study enabled quantitative analysis of the size of various sebum-containing pores before and after sebum extraction. The findings of the present study provided a quantitative basis for the noninvasive 3D evaluation of skin sebum.

5 Conclusion

In conclusion, we used the skin measurement algorithm in the proposed SD-OCT system to evaluate an arbitrary sebum area of the face. OCT images enabled noninvasive measurement of the morphological structures of pores and sebum areas. The obtained MAP image was processed using an ImageJ pore detection algorithm to quantitatively analyze the areas of the selected pores. We also analyzed the areas of nose skin before and after sebum extraction, which further demonstrated the usefulness of OCT as a tool for skin research as it could quantitatively evaluate skin pores and sebum characteristics.

Acknowledgements This research was supported by the MSIT (Ministry of Science and ICT), Korea, under the Innovative Human Resource Development for Local Intellectualization support program (IITP-2023-RS-2022-00156389) supervised by the IITP (Institute for Information & communications Technology Planning & Evaluation). This work was also supported by the Korea Medical Device Development Fund grant funded by the Korea government (the Ministry of Science and ICT, the Ministry of Trade, Industry and Energy, the Ministry of Health & Welfare, the Ministry of Food and Drug Safety) (Project Number: RS-2020-KD000055).

Author contributions HMK and DK designed and performed all experiments. HMK, DK, DS, and SH designed the optical system. DS and S.H. provided programming source code for imaging. HMK and DK analyzed and interpreted the statistical data. SAS, JAL, YK, and HYK helped to interpret the data evaluation from technical point of view. HMK and DK drafted the manuscript. HMK, DKJAL, and SAS edited the manuscript. MJ and JK designed and supervised the entire research, edited the paper, and provided necessary input for all experiments.

Declarations

Conflict of interest The authors declare that they have no known competing financial interests or personal relationships that could have appeared to influence the work reported in this paper.

Funding The authors have not disclosed any funding.

References

1. Li D, Li Z, Zhang J, Li K, Wu S, He Y, Lin Y. Orthogonal-polarization-gating optical coherence tomography for human sweat ducts in vivo. J Biophotonics. 2021;14:e202000432.
2. Maiti R, Duan M, Danby SG, Lewis R, Matcher SJ, Carré MJ. Morphological parametric mapping of 21 skin sites throughout the body using optical coherence tomography. J Mech Behav Biomed Mater. 2020;102:103501.
3. Zhao Q, Dai C, Fan S, Lv J, Nie L. Synergistic efficacy of salicylic acid with a penetration enhancer on human skin monitored by OCT and diffuse reflectance spectroscopy. Sci Rep. 2016;6:1–1.
4. Zhang Q, Whangbo T Skin pores detection for image-based skin analysis. In: Intelligent data engineering and automated learning–IDEAL 2008: 9th international conference Daejeon, South Korea, November 2–5, 2008 Proceedings 9, 2008, pp. 233–40.
5. Yamazaki K, Li E, Miyazawa A, Kobayashi M, Sayo T, Makita S, Takahashi Y, Yasuno Y, Sakai S. Depth-resolved investigation of multiple optical properties and wrinkle morphology in eye-corner areas with multi-contrast Jones matrix optical coherence tomography. Skin Res Technol. 2021;27:435–43.
6. Sun J, Kim S, Lee S, Choi J, Ko S. Automatic facial pore analysis system using multi-scale pore detection. Skin Res Technol. 2017;23:354–62.
7. Kim S, Shin M, Back J, Koh J. Pore volume is most highly correlated with the visual assessment of skin pores. Skin Res Technol. 2014;20:429–34.
8. Jo HY, Yu DS, Oh CH. Quantitative research on skin pore widening using a stereoimage optical topometer and Sebutape®. Skin Res Technol. 2007;13:162–8.
9. Mizukoshi K, Takahashi K. Analysis of the skin surface and inner structure around pores on the face. Skin Res Technol. 2014;20:23–9.
10. Ahn Y, Lee C-Y, Baek S, Kim T, Kim P, Lee S, Min D, Lee H, Kim J, Jung W. Quantitative monitoring of laser-treated engineered skin using optical coherence tomography. Biomed Opt Express. 2016;7:1030–41.
11. Piérard-Franchimont C, Piérard G. Postmenopausal aging of the sebaceous follicle: a comparison between women receiving hormone replacement therapy or not. Dermatology. 2002;204:17–22.
12. Moon J, Yi G, Oh C, Lee M, Lee Y, Kim M. A new technique for three-dimensional measurements of skin surface contours: evaluation of skin surface contours according to the ageing process using a stereo image optical topometer. Physiol Meas. 2002;23:247.
13. Saedi N, Petrell K, Arndt K, Dover J. Evaluating facial pores and skin texture after low-energy nonablative fractional 1440-nm laser treatments. J Am Acad Dermatol. 2013;68:113–8.
14. Cula OG, Dana KJ, Murphy FP, Rao BK. Skin texture modeling. Int J Comput Vis. 2005;62:97–119.
15. Cula OG, Dana KJ Image-based skin analysis. In: Proceedings of texture 2002-the 2nd international workshop on texture analysis and synthesis; 2002, pp. 35–40.
16. Bailey SH, Oni G, Brown SA, Kashefi N, Cheriyan S, Maxted M, Stewart C, Jones C, Maluso P, Kenkel AM. The use of non-invasive instruments in characterizing human facial and abdominal skin. Lasers Surg Med. 2012;44:131–42.
17. Gianeti MD, Maia Campos PM. Efficacy evaluation of a multifunctional cosmetic formulation: the benefits of a combination of active antioxidant substances. Molecules. 2014;19:18268–82.
18. Filoni A, Alaibac M. Reflectance confocal microscopy in evaluating skin cancer: a clinicians's perspective. Front Oncol. 2019;9:1457.
19. Masters BR, So P, Gratton E. Multiphoton excitation fluorescence microscopy and spectroscopy of in vivo human skin. Biophys J. 1997;72:2405–12.
20. Koehler MJ, König K, Elsner P, Bückle R, Kaatz M. In vivo assessment of human skin aging by multiphoton laser scanning tomography. Opt Lett. 2006;31:2879–81.
21. Lacarrubba F, Pellacani G, Gurgone S, Verzì AE, Micali G. Advances in non-invasive techniques as aids to the diagnosis and monitoring of therapeutic response in plaque psoriasis: a review. Int J Dermatol. 2015;54:626–34.

22. Calzavara-Pinton P, Longo C, Venturini M, Sala R, Pellacani G. Reflectance confocal microscopy for in vivo skin imaging. Photochem Photobiol. 2008;84:1421–30.
23. Fujimura T, Haketa K, Hotta M, Kitahara T. Global and systematic demonstration for the practical usage of a direct in vivo measurement system to evaluate wrinkles. Int J Cosmet Sci. 2007;29:423–36.
24. Jacobi U, Chen M, Frankowski G, Sinkgraven R, Hund M, Rzany B, Sterry W, Lademann J. In vivo determination of skin surface topography using an optical 3D device. Skin Res Technol. 2004;10:207–14.
25. Huang D, Swanson EA, Lin CP, Schuman JS, Stinson WG, Chang W, Hee MR, Flotte T, Gregory K, Puliafito CA. Optical coherence tomography. Science. 1991;254:1178–81.
26. Fercher AF. Optical coherence tomography. J Biomed Opt. 1996;1:157–73.
27. Fercher AF, Drexler W, Hitzenberger CK, Lasser T. Optical coherence tomography-principles and applications. Rep Prog Phys. 2003;66:239.
28. Fujimoto JG, Pitris C, Boppart SA, Brezinski ME. Optical coherence tomography: an emerging technology for biomedical imaging and optical biopsy. Neoplasia. 2000;2:9–25.
29. Seong D, Ki W, Kim P, Lee J, Han S, Yi S, Kim HK, Jeon M, Kim J. Virtual intraoperative optical coherence tomography angiography integrated surgical microscope for simultaneous imaging of morphological structures and vascular maps in vivo. Opt Lasers Eng. 2022;151:106943.
30. Považay B, Bizheva K, Hermann B, Unterhuber A, Sattmann H, Fercher AF, Drexler W, Schubert C, Ahnelt P, Mei M. Enhanced visualization of choroidal vessels using ultrahigh resolution ophthalmic OCT at 1050 nm. Opt Express. 2003;11:1980–6.
31. Yarmohammadi A, Zangwill LM, Diniz-Filho A, Suh MH, Manalastas PI, Fatehee N, Yousefi S, Belghith A, Saunders LJ, Medeiros FA. Optical coherence tomography angiography vessel density in healthy, glaucoma suspect, and glaucoma eyes. Invest Ophthalmol Visual Sci. 2016;57:OCT451–9.
32. Djalilian HR, Ridgway J, Tam M, Sepehr A, Chen Z, Wong BJ. Imaging the human tympanic membrane using optical coherence tomography in vivo. Otol Neurotol Off Publ Am Otol Soc Am Neurotol Soc Eur Acad Otol Neurotol. 2008;29:1091.
33. Bibas AG, Podoleanu AG, Cucu RG, Dobre GM, Odell E, Boxer AB, O'Connors AF, Gleeson MJ. Optical coherence tomography in otolaryngology: original results and review of the literature. Lasers Surg Adv Charact Ther Syst XIV. 2004;5312:190–5.
34. Seong D, Kwon J, Jeon D, Wijesinghe RE, Lee J, Ravichandran NK, Han S, Lee J, Kim P, Jeon M. In situ characterization of micro-vibration in natural latex membrane resembling tympanic membrane functionally using optical doppler tomography. Sensors. 2019;20:64.
35. Seong D, Lee C, Jeon M, Kim J. Doppler optical coherence tomography for otology applications: from phantom simulation to in vivo experiment. Appl Sci. 2021;11:5711.
36. Hsieh Y-S, Ho Y-C, Lee S-Y, Chuang C-C, Tsai J-C, Lin K-F, Sun C-W. Dental optical coherence tomography. Sensors. 2013;13:8928–49.
37. Lenton P, Rudney J, Chen R, Fok A, Aparicio C, Jones RS. Imaging in vivo secondary caries and ex vivo dental biofilms using cross-polarization optical coherence tomography. Dent Mater. 2012;28:792–800.
38. Kim Y, Jung G-I, Jeon D, Wijesinghe RE, Seong D, Lee J, Do WJ, Kwon S-M, Lee JH, Hwang JH. Non-invasive optical coherence tomography data-based quantitative algorithm for the assessment of residual adhesive on bracket-removed dental surface. Sensors. 2021;21:4670.
39. Lee J, Lee S-Y, Han S, Seong D, Wijesinghe RE, Kim P, Jeon M, Jung H-Y, Kim J. Multi-directional morphological assessment of single bacterial colonies through non-invasive optical imaging. Ann Biomed Eng. 2020;48:3014–23.
40. Saleah SA, Lee S-Y, Wijesinghe RE, Lee J, Seong D, Ravichandran NK, Jung H-Y, Jeon M, Kim J. Optical signal intensity incorporated rice seed cultivar classification using optical coherence tomography. Comput Electron Agric. 2022;198:107014.
41. Welzel J, Lankenau E, Birngruber R, Engelhardt R. Optical coherence tomography of the human skin. J Am Acad Dermatol. 1997;37:958–63.
42. Podoleanu AG, Rogers JA, Jackson DA, Dunne S. Three dimensional OCT images from retina and skin. Opt Express. 2000;7:292–8.
43. Greaves NS, Benatar B, Whiteside S, Alonso-Rasgado T, Baguneid M, Bayat A. Optical coherence tomography: a reliable alternative to invasive histological assessment of acute wound healing in human skin? Br J Dermatol. 2014;170:840–50.
44. Liu L, Gardecki JA, Nadkarni SK, Toussaint JD, Yagi Y, Bouma BE, Tearney GJ. Imaging the subcellular structure of human coronary atherosclerosis using micro–optical coherence tomography. Nat Med. 2011;17:1010–4.
45. Yu X, Xiong Q, Luo Y, Wang N, Wang L, Tey HL, Liu L. Contrast enhanced subsurface fingerprint detection using high-speed optical coherence tomography. IEEE Photonics Technol Lett. 2016;29:70–3.
46. Luo Y, Cui D, Yu X, Bo E, Wang X, Wang N, Braganza CS, Chen S, Liu X, Xiong Q. Endomicroscopic optical coherence tomography for cellular resolution imaging of gastrointestinal tracts. J Biophotonics. 2018;11:e201700141.
47. Seong D, Han S, Jeon D, Kim Y, Wijesinghe RE, Ravichandran NK, Lee J, Lee J, Kim P, Lee D-E. Dynamic compensation of path length difference in optical coherence tomography by an automatic temperature control system of optical fiber. IEEE Access. 2020;8:77501–10.
48. Saleah SA, Seong D, Han S, Wijesinghe RE, Ravichandran NK, Jeon M, Kim J. Integrated quad-scanner strategy-based optical coherence tomography for the whole-directional volumetric imaging of a sample. Sensors. 2021;21:1305.
49. Abràmoff MD, Magalhães PJ, Ram SJ. Image processing with ImageJ. Biophotonics Int. 2004;11:36–42.
50. Ding B, Wang H, Chen P, Zhang Y, Liang R, Liu Y. Subcutaneous sweat pore estimation from optical coherence tomography. IET Image Proc. 2021;15:3267–80.
51. Kislevitz M, Akgul Y, Wamsley C, Hoopman J, Kenkel J. Use of optical coherence tomography (OCT) in aesthetic skin assessment—a short review. Lasers Surg Med. 2020;52:699–704.
52. Ohmi M, Tanigawa M, Wada Y, Haruna M. Dynamic analysis for mental sweating of a group of eccrine sweat glands on a human fingertip by optical coherence tomography. Skin Res Technol. 2012;18:378–83.
53. Flament F, Francois G, Qiu H, Ye C, Hanaya T, Batisse D, Cointereau-Chardon S, Seixas MDG, Dal Belo SE, Bazin R. Facial skin pores: a multiethnic study. Clin Cosmet Investig Dermatol. 2015;8:85–93.
54. Seong D, Jeon D, Wijesinghe RE, Park K, Kim H, Lee E, Jeon M, Kim J. Ultrahigh-speed spectral-domain optical coherence tomography up to 1-mhz a-scan rate using space–time-division multiplexing. IEEE Trans Instrum Meas. 2021;70:1–8.